ACS APPLIED MATERIALS & INTERFACES

www.acsami.org Research Article

Solution-Processed Polymeric Thin Film as the Transparent Electrode for Flexible Perovskite Solar Cells

Tao Zhu, Yongrui Yang, Xiang Yao, Zixu Huang, Lei Liu, Wenping Hu, and Xiong Gong*

Cite This: https://dx.doi.org/10.1021/acsami.9b22891 Read Online

ACCESS | Metrics & More | Article Recommendations

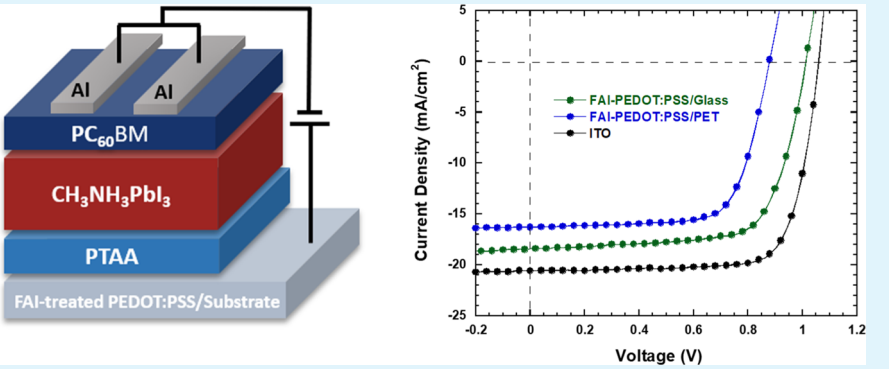

ABSTRACT: In the past decade, perovskite solar cells (PSCs) were arising as a new generation of low-cost solar technology for renewable energy generation. More than 25% of power conversion efficiency (PCE) was reported from PSCs on the rigid indium tin oxide (ITO)/glass electrode. However, PSCs fabricated on flexible solution-processed transparent electrodes have still been a challenge to date. In this work, we report a solution-processed transparent polymeric thin film as the electrode for flexible solution-processed PSCs. The solution-processed polymeric thin film exhibits superior optical transparency and decent electrical conductivity. As compared with a PCE of 16.60% from PSCs on the ITO/glass substrate, PSCs on the solution-processed transparent polymeric electrode/glass substrate exhibit a PCE of 13.36% and PSCs on the solution-processed transparent polymeric thin-film/polyethylene terephthalate flexible substrate possess a PCE of 10.16%. Systematic studies demonstrate that poor electrical conductivity of the solution-processed transparent polymeric electrode and serious interfacial charge carrier recombination are responsible for low PCEs. Nevertheless, our results demonstrate that we provide a facile route to develop flexible PSCs by utilization of solution-processed polymeric thin films as the transparent electrodes.

KEYWORDS: *polymeric thin-film, transparent electrode, flexible perovskite solar cells, high electrical conductivity, device performance*

INTRODUCTION

In the past decade, both academic and industrial sectors have paid great attention to perovskite solar cells (PSCs) due to the advanced features such as superior optoelectronic properties of perovskite materials and low-cost fabrication processes of PSCs.[1−6] Over 25% of power conversion efficiency (PCE) was recently reported from PSCs.[7] In such rapidly developed PSCs, either indium tin oxide (ITO)- or fluorine-doped tin oxide (FTO)-coated glass was used as the transparent electrode.[8−14] However, both ITO- and FTO-coated glass substrates possess several drawbacks such as rigidity and frangibility, which certainly limit the application of PSCs into flexible, portable, and wearable electronics.[15,16] In addition, the scarcity of the indium element and the high-temperature sintering process to produce either ITO- or FTO coated glass substrates add to the cost of PSCs. Thus, PSCs on the solution-processed transparent flexible electrodes would possess great potential in various practice applications.[16]

To date, silver nanowires (AgNWs),[17] multiwalled carbon nanotubes,[18] and semiconducting polymers[19,20] have been developed to substitute the ITO or FTO as the transparent electrodes. AgNWs possess superior electrical conductivity, but the reaction of Ag^+ ions with halogen ions (I^- or Cl^-) from perovskite materials degrade the electrical conductivity of AgNWs dramatically.[21,22] MWNTs could be solution-processed, but exhibit a poor optical density,[23] which certainly

Received: December 22, 2019
Accepted: March 10, 2020
Published: March 10, 2020

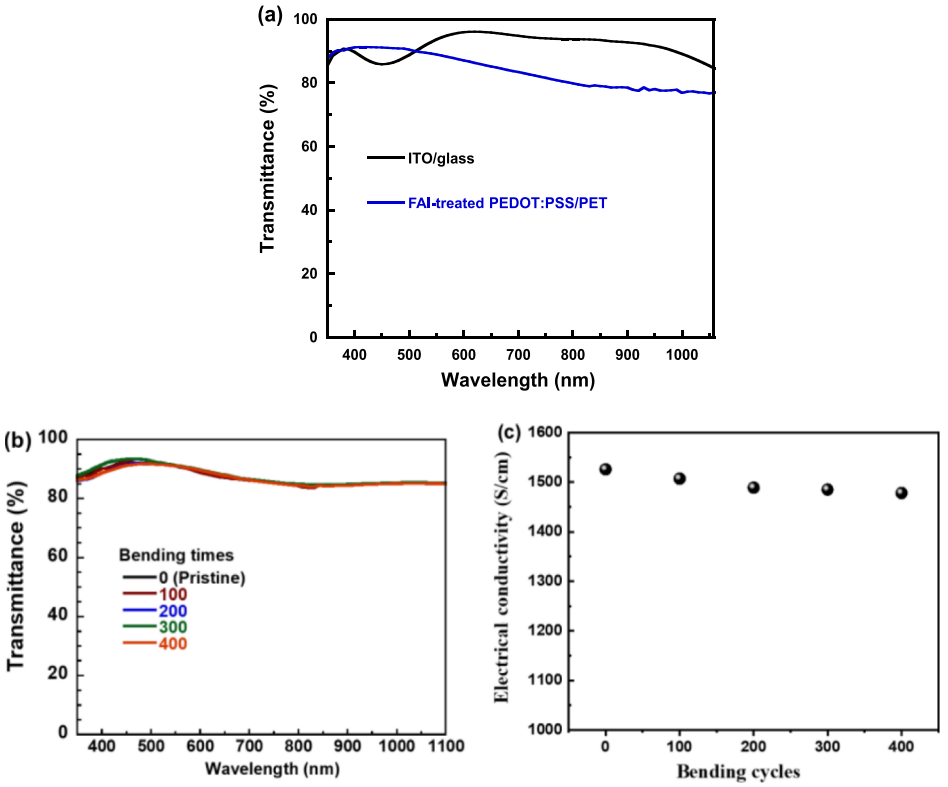

Figure 1. (a) Transmittance spectra of the FAI-treated PEDOT:PSS thin film/PET substrate and the ITO/glass substrate. (b) Transmittances and (c) electrical conductivities of FAI-treated PEDOT:PSS thin films under different bending cycles.

restricts the perovskite photoactive layer to absorb the photon for generating large photocurrent from PSCs. Semiconducting polymers are alternatives as the transparent electrode for flexible PSCs by virtue of their excellent features such as solution-processable, cost-effective, lightweight, superior mechanical flexibility, and compatibility with plastic substrates. In the past years, poly(3,4-ethylenedioxythiophene):poly(styrene sulfonate) (PEDOT:PSS) thin films have drawn great attention in the society of flexible electronics. Much effort have been made to enhance the electrical conductivity, and dramatically boosted electrical conductivity of PEDOT:PSS thin films indeed were observed.[24−26] For example, Wang et al.[25] observed 2980 S/cm electrical conductivity from PEDOT:PSS thin film treated by a super-acid. Kim et al.[26] reported an electrical conductivity of 4380 S/cm from PEDOT:PSS thin film treated by sulfuric acid. However, PEDOT:PSS thin films treated with strong acids would adversely affect both underneath and above layers, hampering their applications in flexible electronics.

Here, we exemplify the application of thin-film iodide (FAI) as a non-acidic agent to treat a PEDOT:PSS thin film. It is found that the electrical conductivity of PEDOT:PSS thin film is increased by 4 orders of magnitude as compared with that of pristine PEDOT:PSS thin film. Moreover, the FAI-treated PEDOT:PSS thin films exhibit superior optical transparency in the whole visible range. The PSCs on the FAI-treated PEDOT:PSS transparent electrode coated on polyethylene terephthalate (PET) flexible substrate exhibit over 10% PCE, which is slightly lower than that on the glass rigid substrate. Systematic studies indicate that poor electrical conductivity of the solution-processed transparent polymeric electrode and serious interfacial charge carrier recombination are responsible for low PCEs of flexible PSCs.

EXPERIMENTAL SECTION

Materials. PEDOT:PSS (Clevios PH1000) was purchased from Heraeus Precious Metal, North America., Inc. [6,6]-phenyl-C61-butyric acid methyl ester ($PC_{61}BM$) was bought from Solenne BV. Lead iodide (PbI_2) was purchased from Alfa Aesar. Poly[bis(4-phenyl)(2,4,6-trimethylphenyl)amine] (PTAA), *N*,*N*-dimethylformamide (DMF, anhydrous, ≥99.9%), isopropyl alcohol (anhydrous, ≥99%), ethyl alcohol (≥99.9%), and chlorobenzene (anhydrous, ≥99.9%) were purchased from Sigma-Aldrich. Formamidinium iodide (FAI) and methylammonium iodide (MAI) were synthesized in our laboratory.[6,27]

FAI-Treated PEDOT:PSS Thin Film Preparation. Pristine PEDOT:PSS solution (Clevios PH1000) was spin-coated on the precleaned and UV-treated PET or glass substrates, followed with thermal annealing on the hotplate at 140 °C for 10 min (min). Afterward, 100 μL of FAI DMF solution was dropped upon the preheated PEDOT:PSS thin films. Finally, the excess FAI salts on the surface of PEDOT:PSS thin films were rinsed several times by deionized water and isopropanol.

Thin Film Characterizations. A profilometer (Bruker DektakXT Stylus) was used to measure the thicknesses of all thin films under the scan rate of 0.03 mm/s. Sheet resistance of thin films was measured by the traditional van der Pauw four-point probing method. A Lambda 900 UV−Vis−NIR spectrophotometer (PerkinElmer, Waltham, MA, USA) was used to characterize the transmittance spectra of all thin films. The contact angles of either the FAI-treated PEDOT:PSS thin film or the ITO substrate were measured on angle analysis equipment from AST Products' VCA Optima. Scanning electron microscopy (SEM) images were obtained using the scanning electron microscope (S-2600N).

Fabrication and Characterization of PSCs. PSCs were fabricated with a device configuration of PET (or glass)/FAI-treated PEDOT:PSS/PTAA/$CH_3NH_3PbI_3$/$PC_{61}BM$/Al and with a typical standard device configuration of ITO/PTAA/$CH_3NH_3PbI_3$/$PC_{61}BM$/Al. The thickness of the FAI-treated PEDOT:PSS thin film is measured to be ∼40 nm. A PTAA hole extraction layer was

https://dx.doi.org/10.1021/acsami.9b22891
ACS Appl. Mater. Interfaces XXXX, XXX, XXX−XXX

prepared from 5 mg/mL in toluene by spin coating at 6000 rpm for 25 s (s) with a thickness of 35 nm. The PbI_2 layer was cast on the preheated (80 °C) PET (or glass)/FAI-treated PEDOT:PSS/PTAA or ITO/PTAA from the PbI_2 solution (DMF, 400 mg mL^{-1}) at 6000 rpm for 20 s, then the substrates were placed on a hotplate at 80 °C for 10 min. The MAI layer was then cast on the top of the cooled PbI_2 layer from the MAI precursor ethanol solution (40 mg mL^{-1}) at 6000 rpm for 35 s, followed by thermal annealing at 100 °C for 90 min to form $CH_3NH_3PbI_3$ thin films. The $PC_{61}BM$ layers were then spin-coated on the top of the cooled perovskite layers at 1000 rpm for 35 s. The aluminum (Al) cathode was thermally evaporated under high vacuum (10^{-6} mbar) with a thickness of 100 nm. The device area is measured to be 45 mm^2. The performance of PSCs was characterized under an AM 1.5 G solar simulator (Newport, 91160-1000); white light intensity was calibrated by a mono-silicon detector (with KG-5 visible color filter) of National Renewable Energy Laboratory. The current density versus voltage (J–V) characteristics of PSCs under white light illumination and in dark were obtained by using a Keithley 2400 source meter. The external quantum efficiency (EQE) spectra of the PSCs were measured through the solar cell quantum efficiency measurement system (QEX10) with a 300 W steady-state Xenon lamp as the light source from PV Measurement, Inc. The impedance spectrum (IS) of all solar cells were obtained using an HP 4194A impedance/gain-phase analyzer under dark condition.

RESULTS AND DISCUSSION

Figure 1a presents the transmittance spectra of the FAI-treated PEDOT:PSS thin film/PET and the ITO/glass. Compared to the transparency of the ITO/glass electrode, the FAI-treated PEDOT:PSS thin film/PET exhibits slightly less transmittance, but still possesses over 85% transmittance from 350 to 550 nm and around 75% transmittance from 550 to 900 nm. Therefore, the FAI-treated PEDOT:PSS thin film/PET has good optical transparency used as the transparent electrode.

The electrical conductivity of pristine PEDOT:PSS thin film is about ~0.3 S/cm, but it is found that the electrical conductivities of treated PEDOT:PSS thin films are boosted to over 1000 S/cm at the concentration of FAI at 0.1 M.[28] The realigned orientation of the PEDOT structure is responsible for such enhanced electrical conductivity.[28] To further optimize the electrical conductivities, the FAI-treated PEDOT:PSS thin films are thermally annealed at different temperatures.[28] The electrical conductivities of the FAI-treated PEDOT:PSS thin films are increased drastically with the increment of thermal annealing temperature in the range of 80–140 °C. The optimal electrical conductivity reaches 1562 ± 36 S/cm as the annealing temperature is at 140 °C. Such increased electrical conductivity is due to the fact that the movement of PEDOT chains is promoted as the increased thermal energy, resulting in more aligned PEDOT chains, boosting the electrical conductivity.[28] However, further increasing the annealing temperature over 140 °C, the electrical conductivity is decreased, which is attributed to the degradation of PET substrates as the annealing temperature above 140 °C.[29,30]

In addition, it is also found that the FAI-treated PEDOT:PSS thin film still possesses good transparency and electrical conductivity after it has had 400 times bending cycle as shown in Figure 1b,c.

It has been reported that the PEDOT chains are hydrophobic, which are bound to the hydrophilic PSS chains, so they are well stabilized in water. However, as temperature increased, the PEDOT chains and PSS chains could move. Once the PEDOT:PSS surface was treated by FAI in a DMF solvent, at high temperature (over 100 °C), the I^- in FAI would bind to PEDOT:PSS chains and FA^+ in FAI would bind to PSS chains. As a result, the PEDOT chains would be isolated from PSS chains, consequently exhibiting hydrophobic properties. Figure 2a,b presents the static contact angles of

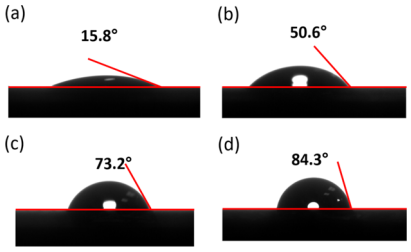

Figure 2. Contact angles of water on the surfaces of (a) PEDOT:PSS thin film/silicon substrate, (b) FAI-treated PEDOT:PSS thin film/silicon substrate, (c) PTAA thin film/ITO/glass, and (d) PTAA thin film/FAI-treated PEDOT:PSS/glass.

water on the surfaces of the PEDOT:PSS/silicon and FAI-treated PEDOT:PSS/silicon substrates, respectively. The contact angle observed from the PEDOT:PSS/silicon substrate is 15.8°, whereas the contact angle observed from the FAI-treated PEDOT:PSS/silicon substrate is enlarged to 50.6°. Such enlarged contact angle indicates that the FAI-treated PEDOT:PSS thin layer is more hydrophobic than pristine PEDOT:PSS, which is consistent with our above hypothesis. Moreover, the hydrophobic properties of the PTAA layer on either ITO/glass or FAI-treated PEDOT:PSS/glass substrate are investigated and the results are shown in Figure 2c,d. Interestingly, a slightly enlarged contact angle (84.3°) is observed for the PTAA/FAI-treated PEDOT:PSS/glass substrate compared to that (73.2°) observed for the PTAA/ITO/glass substrate. It was reported that the nonwetting property of the PTAA layer is favorable for $CH_3NH_3PbI_3$ to form large grain size with fewer grain boundaries,[31] giving rise to enhanced charge-carrier mobility, and consequently, boosted short-circuit current density (J_{SC}) is expected from the PSCs.[32]

SEM was conducted to confirm the above hypothesis. Figure 3 displays the top-view SEM images of the $CH_3NH_3PbI_3$ active

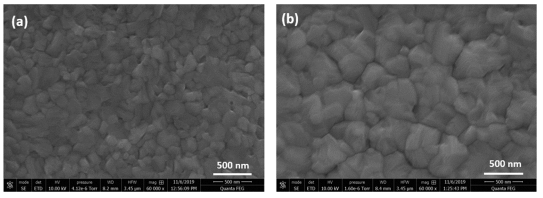

Figure 3. Top-view SEM images of $CH_3NH_3PbI_3$ thin films on the top of (a) PTAA/ITO thin film and (b) PTAA/FAI-treated PEDOT:PSS thin film.

layer on either the PTAA/ITO/glass or PTAA/FAI-treated PEDOT:PSS/glass substrates. The crystal grain size increases substantially from ~100 nm (on PTAA/ITO/glass) to over 400 nm (PTAA/FAI-treated PEDOT:PSS/glass), confirming that the diminished surface tension of PTAA on the FAI-treated PEDOT:PSS thin layer has exerted a crucial impact on the nucleation and crystal growth processes of the $CH_3NH_3PbI_3$ active layer. It should be noted that the grain size of perovskite we observed is smaller than the reported one,[33,34] which is probably because lower concentration of

https://dx.doi.org/10.1021/acsami.9b22891
ACS Appl. Mater. Interfaces XXXX, XXX, XXX–XXX

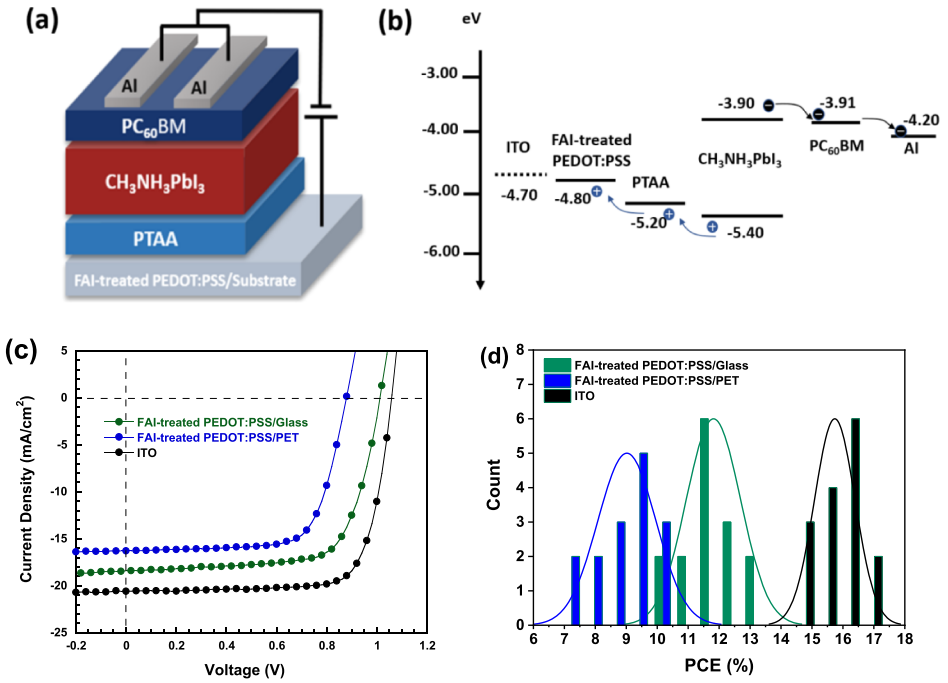

Figure 4. (a) Device configuration of PSCs, (b) LUMO and HOMO energy levels of PTAA, $CH_3NH_3PbI_3$, $PC_{60}BM$, and the work functions of the FAI-treated PEDOT:PSS thin film and aluminum electrodes, respectively. (c) $J-V$ characteristics of PSCs with different transparent electrodes (ITO/glass, the FAI-treated PEDOT:PSS thin films on glass, and PET substrates) under white light illumination. (d) PCE statistics of the PSCs with different transparent electrodes (ITO/glass, the FAI-treated PEDOT:PSS thin films on glass, and PET substrates).

Table 1. Device Performance Parameters of PSCs[a]

Substrates	J_{SC}[a] (mA/cm^2)>	J_{SC}[b] (mA/cm^2)>	V_{OC} (V)	FF (%)	PCE (%)	R_{Sh} (Ω cm^2)	R_S (Ω cm^2)
ITO/glass	20.58	19.15	1.06	76	16.60	2624	4.20
FAI-PEDOT:PSS/glass	18.40	17.53	1.02	71	13.36	1354	5.62
FAI-PEDOT:PSS/PET	16.75	16.12	0.96	63	10.16	1160	5.95

[a] J_{SC} from $J-V$ characteristics. [b] J_{SC} from the integration of the EQE spectra.

MAI was used to prepare the $CH_3NH_3PbI_3$ thin film under this investigation.

The device structure of PSCs under this investigation is shown in Figure 4a. The lowest unoccupied molecular orbital (LUMO) and the highest occupied molecular orbital (HOMO) energy levels of PTAA, $CH_3NH_3PbI_3$, $PC_{60}BM$, and the work functions of FAI-treated PEDOT:PSS and Al electrodes are displayed in Figure 4b, where the FAI-treated PEDOT:PSS thin film acts as the transparent anode, PTAA acts as a hole extraction layer, $PC_{61}BM$ acts as the electron extraction layer, and aluminum (Al) serves as the cathode. It has been reported that the interfacial energy barrier is very essential to the device performance.[35] To confirm the HOMO energy level of the FAI-treated PEDOT:PSS thin film, cyclic voltammetry measurement is conducted. Based on the oxidation and reduction potentials, the LUMO energy level of the FAI-treated PEDOT:PSS thin film is estimated to be −4.80 eV,[28,36] which is close to the work function of ITO (−4.70 eV), indicating that the FAI-treated PEDOT:PSS thin film possesses similar work function as that of ITO electrode. Figure 4c displays the $J-V$ characterization of PSCs fabricated on different transparent electrodes. The device performance of PSCs is summarized in Table 1. The PSCs fabricated on the ITO/glass electrode exhibit an open-circuit voltage (V_{OC}) of 1.06 V, a J_{SC} of 20.58 mA cm^{-2}, a fill factor (FF) of 76%, and with a corresponding PCE of 16.60%. The PSCs fabricated on the FAI-treated PEDOT:PSS/glass electrode show a V_{OC} of 1.02 V, a J_{SC} of 18.40 mA cm^{-2}, a FF of 71%, with a corresponding PCE of 13.36%, which is slightly lower than that of the PSCs fabricated on the ITO/glass electrode. The PSCs fabricated on the flexible FAI-treated PEDOT:PSS/PET electrode show a V_{OC} of 0.96 V, a J_{SC} of 16.75 mA cm^{-2}, a FF of 63%, with a corresponding PCE of 10.16%, which is lower than that of the FAI-treated PEDOT:PSS thin film on the glass substrate.

The PCE performance histograms (gathered from 15 identical devices) and the corresponding Gaussian fit for the respective PSCs are shown in Figure 4d. Clearly, the distributions of PCEs from PSCs fabricated on different transparent electrodes, ITO/glass, the FAI-treated PEDOT:PSS thin film/glass, and the FAI-treated PEDOT:PSS thin film/PET substrates are similar. These results further demonstrate that the FAI-treated PEDOT:PSS thin film/PET substrate possesses good optoelectrical and mechanical properties for flexible electronics.

It is noted that larger crystals are observed from the $CH_3NH_3PbI_3$ thin films on the FAI-treated PEDOT:PSS/glass substrate (Figure 3), but lower J_{SC} values are obtained from the PSCs on either the FAI-treated PEDOT:PSS/PET flexible substrate or the FAI-treated PEDOT/glass rigid substrates. Typically, $CH_3NH_3PbI_3$ thin films with larger crystals could generate higher J_{SC} in the PSCs on ITO/glass substrate.[6] However, in this study, an inferior charge transport originated

https://dx.doi.org/10.1021/acsami.9b22891
ACS Appl. Mater. Interfaces XXXX, XXX, XXX−XXX

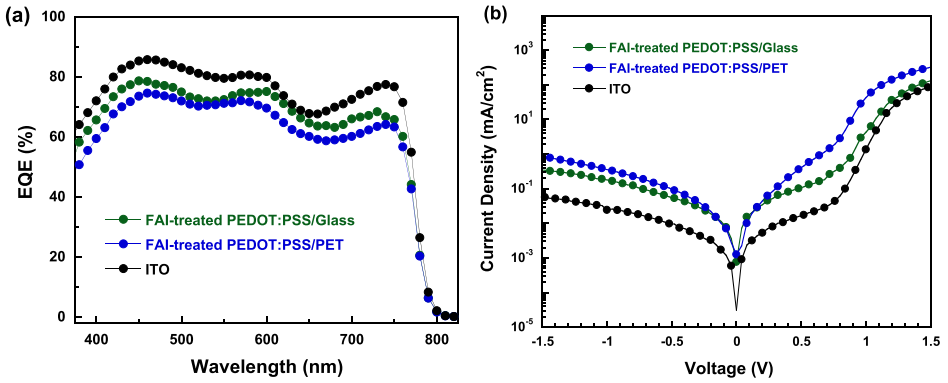

Figure 5. (a) EQE spectra of PSCs and (b) $J-V$ characteristics of PSCs with different transparent electrodes (ITO/glass, the FAI-treated PEDOT:PSS thin films on glass, and PET substrates) measured in dark.

from the poor electrical conductivity of the FAI-treated PEDOT:PSS is likely responsible for the reduced J_{SC}.

In order to understand the inferior device performance observed from PSCs with the FAI-treated PEDOT:PSS as the electrode, the shunt resistance and series resistance of PSCs are investigated. J is described as[37]

$$J = J_0\left[\exp\left(\frac{q(V - R_S AJ)}{nkT}\right) - 1\right] + \frac{V - R_S AJ}{R_{SH}A} - J_{ph}(V) \quad (1)$$

which is based on the model of $J-V$ characteristics of PSCs with an equivalent circuit. Under the open-circuit condition, where $J = 0$ and $J_{ph} = J_{SC}$, the above eq 1 is rearranged to

$$V_{OC} \approx \frac{nkT}{q} \ln\left(\frac{J_{SC}}{J_0}\right) \quad (2)$$

where J_0 is reverse saturation current governed by diffusion and recombination of charge carriers, n is ideal factor, k is Boltzman's constant, T is absolute temperature, q is the elementary electron charge, J_{ph} is the photocurrent, V is an applied voltage, and A is the work area. Both shunt resistance (R_{SH}) and series resistance (R_S) of PSCs are estimated from the reciprocal of the slopes of the $J-V$ curves under the short-circuit and open-circuit conditions, respectively. The results are summarized in Table 1. An R_S of 4.20 Ω cm^2 is observed from the PSCs on the ITO/glass rigid electrode, whereas an R_S of 5.62 Ω cm^2 is observed from the PSCs on the flexible FAI-treated PEDOT:PSS/PET electrode and an R_S of 5.95 Ω cm^2 is observed from PSCs on the FAI-treated PEDOT:PSS/glass electrode. Such enlarged R_S values are originated from the larger contact resistance and lower electrical conductivity of the FAI-treated PEDOT:PSS thin film. The smaller R_{SH} of 1160 Ω cm^2 from the PSCs on the flexible FAI-treated PEDOT:PSS/PET electrode indicates that the current leakages are responsible for the reduced J_{SC}. As a result, lower J_{SC}, and consequently smaller PCE values are observed from the PSCs on the flexible FAI-treated PEDOT:PSS/PET electrode. These results are in good agreement with those observed from the $J-V$ characteristics.

The EQE spectra of PSCs are displayed in Figure 5a. The PSCs with the FAI-treated PEDOT:PSS/PET electrode exhibit a lower EQE than those with the ITO/glass electrode, which is ascribed to the transmittance losses of the FAI-treated PEDOT:PSS thin film in the visible region (Figure 1). Moreover, compared with the electrical conductivity (~6000 S/cm) of the ITO/glass substrates, the relatively poor electrical conductivity (~1500 S/cm) of the FAI-treated PEDOT:PSS thin film is also responsible for lower EQE values of the PSCs on the FAI-treated PEDOT:PSS/PET electrode.[38] The integrated J_{SC} values of 19.15 and 16.12 mA/cm^2 for the PSCs on the ITO/glass electrode and on the FAI-treated PEDOT:PSS/PET electrode. These integrated J_{SC} values are in good agreement with those from the $J-V$ characteristics (Figure 4c).

Figure 5b exhibits the $J-V$ characteristics of PSCs measured in dark. The dark current densities of the PSCs with the flexible FAI-treated PEDOT:PSS/PET electrode and the PSCs with the FAI-treated PEDOT:PSS/glass electrode are approximatively ten times larger than those on the ITO/glass rigid electrode, which further indicates that the PSCs with the flexible FAI-treated PEDOT:PSS/PET electrode and the PSCs with the FAI-treated PEDOT:PSS/glass electrode possess enlarged leakage current densities as compared with those with the ITO/glass rigid electrode. Such high leakage current would generate in shunt-flow instead of flowing through PSCs, resulting in lower J_{SC}. Based on eq 2, the enlarged dark current density would result in a slightly lower V_{OC} for the PSCs with the flexible FAI-treated PEDOT:PSS/PET electrode and the PSCs with the FAI-treated PEDOT:PSS/glass electrode.

Both $J-V$ curves in dark and PL results are consistent with the $J-V$ characteristics (Figure 4c), where the V_{OC} values of the PSCs with the flexible FAI-treated PEDOT:PSS/PET electrode and the PSCs with the FAI-treated PEDOT:PSS/glass electrode are 0.96 and 1.02 V, respectively, whereas the V_{OC} of the PSCs with the ITO/glass is 1.06 V.

Impedance spectroscopy (IS) is performed to explore the electric properties of PSCs which cannot be investigated by direct current measurement. Figure 6 presents the IS spectra of PSCs. The R_S consists of the sheet resistance (R_{sheet}) and the charge-transport resistance (R_{CT}) at the interface between the charge carrier extraction layer and the electrodes, the interface between the charge extraction layer and perovskite layer, as well as inside perovskite thin-film.[39,40] Enhanced R_{CT} values of 1325 and 1065.3 Ω are observed for the PSCs with the flexible FAI-treated PEDOT:PSS/PET electrode and the PSCs with the FAI-treated PEDOT:PSS/glass electrode, respectively. Both of them are much higher than that (842 Ω) of the PSCs with the ITO/glass electrode. These results indicate an inferior charge transport at the interfacial boundaries of PSCs.[41] As a result, the PSCs with the flexible FAI-treated

https://dx.doi.org/10.1021/acsami.9b22891
ACS Appl. Mater. Interfaces XXXX, XXX, XXX−XXX

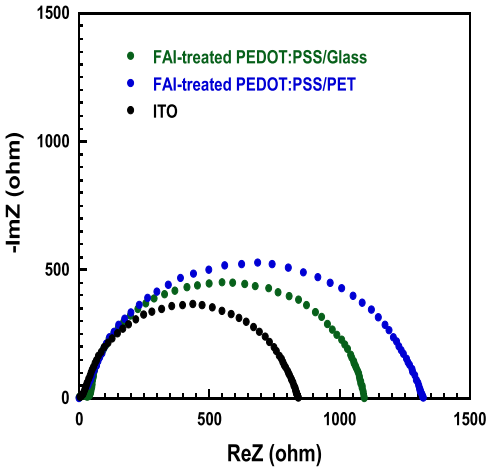

Figure 6. Nyquist plot of PSCs with different transparent electrodes (ITO/glass, the FAI-treated PEDOT:PSS thin films on glass, and PET substrates) measured in dark.

PEDOT:PSS/PET electrode exhibit lower J_{SC}, and consequently, lower PCE.

To further investigate the roles of the interfacial layer in PSCs, light intensity dependence tests of J_{SC} and V_{OC} were performed to evaluate the impact of interface charge carrier recombination within PSCs.[42−44] As shown in Figure 7a, the PSCs with either the FAI-treated PEDOT:PSS electrode (either PET or glass substrates) or the ITO/glass electrode exhibit a power-law dependence of J_{SC} on the light intensity. The J_{SC} can be correlated with the light intensity by $J_{SC} \propto I^{\alpha}$,[45] where I is the light intensity and α is the coefficient.[45] An α of 0.940 is observed from the PSCs with the ITO/glass electrode, and α values of 0.879 and 0.887 are observed from the PSCs with the flexible FAI-treated PEDOT:PSS/PET electrode and the PSCs with the FAI-treated PEDOT:PSS/glass electrode, respectively. The smaller α value indicates that a stronger interface charge carrier (bimolecular) recombination process takes place in the PSCs with the flexible FAI-treated PEDOT:PSS/PET electrode.[32]

Figure 7b displays the light intensity dependence of V_{OC}. Under the open-circuit condition, V_{OC} could be correlated with the light intensity, described by $V_{OC} = n\frac{KT}{q}\ln(I)$,[46,47] where k is the Boltzmann constant, T is the temperature in Kelvin, and q is the elementary charge. As n = 1, the bimolecular recombination is dominated in solar cells, whereas as n = 2, the monomolecular recombination is dominated in solar cells.[46,47] The slopes of $1.92kT/q$ and $1.80kT/q$ are observed from the PSCs with the flexible FAI-treated PEDOT:PSS/PET electrode and the PSCs with the FAI-treated PEDOT:PSS/glass electrode, respectively. Whereas a slope of $1.38kT/q$ is observed from the PSCs with the ITO/glass electrode. A slope close to 2 indicates that a stronger monomolecular charge recombination process takes place in the PSCs with the FAI-treated PEDOT:PSS electrode.[32,46] Thus, the PSCs with the FAI-treated PEDOT:PSS electrode exhibit lower J_{SC} and lower PCE.

CONCLUSIONS

In summary, we demonstrated a simple yet effective method to fabricate flexible PSCs on a solution-processed polymeric thin film as the transparent electrode. The PSCs fabricated on the above solution-processed transparent electrode exhibited slightly lower PCE as compared with that on a rigid electrode. Systematic studies demonstrated that poor electrical conductivity of the solution-processed transparent electrode and serious interfacial charge carrier recombination are responsible for low PCE of flexible PSCs. However, our results demonstrated that we provided a facile route to develop flexible PSCs by utilization of solution-processed polymeric thin film as the transparent electrode.

AUTHOR INFORMATION

Corresponding Author

Xiong Gong − *Department of Polymer Engineering, College of Polymer Science and Polymer Engineering, The University of, Akron, Ohio 44325, United States;* orcid.org/0000-0001-6525-3824; Email: xgong@uakron.edu; Fax: (330) 9723406

Authors

Tao Zhu − *Department of Polymer Engineering, College of Polymer Science and Polymer Engineering, The University of, Akron, Ohio 44325, United States*

Yongrui Yang − *Department of Polymer Engineering, College of Polymer Science and Polymer Engineering, The University of, Akron, Ohio 44325, United States*

Xiang Yao − *Tianjin Key Laboratory of Molecular Optoelectronic Sciences, School of Science, Tianjin University and Collaborative Innovation Centre of Chemical Science and Engineering, Tianjin 300072, P. R. China*

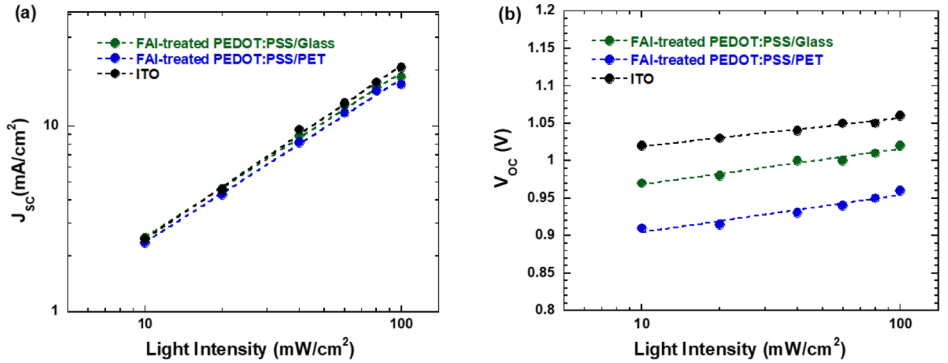

Figure 7. Light intensity dependences of the steady-state (a) J_{SC} and (b) V_{OC} of PSCs with different transparent electrodes (ITO/glass, the FAI-treated PEDOT:PSS thin films on glass, and PET substrates).

https://dx.doi.org/10.1021/acsami.9b22891
ACS Appl. Mater. Interfaces XXXX, XXX, XXX−XXX

Zixu Huang − *Department of Polymer Engineering, College of Polymer Science and Polymer Engineering, The University of, Akron, Ohio 44325, United States*
Lei Liu − *Department of Polymer Engineering, College of Polymer Science and Polymer Engineering, The University of, Akron, Ohio 44325, United States*
Wenping Hu − *Tianjin Key Laboratory of Molecular Optoelectronic Sciences, School of Science, Tianjin University and Collaborative Innovation Centre of Chemical Science and Engineering, Tianjin 300072, P. R. China;* orcid.org/0000-0001-5686-2740

Complete contact information is available at: https://pubs.acs.org/10.1021/acsami.9b22891

Notes

The authors declare no competing financial interest.

■ ACKNOWLEDGMENTS

The authors at the University of Akron thank National Science Foundation (EECs 1351785 and EECs 1903303) and Air Force Office of Scientific Research (AFOSR) (through the Organic Materials Chemistry Program, grant number: FA9550-15-1-0292, Program Manager, Dr. Kenneth Caster) for financial supports.

■ REFERENCES

(1) Kojima, A.; Teshima, K.; Shirai, Y.; Miyasaka, T. Organometal Halide Perovskites as Visible-Light Sensitizers for Photovoltaic Cells. *J. Am. Chem. Soc.* **2009**, *131*, 6050−6051.
(2) Wehrenfennig, C.; Eperon, G. E.; Johnston, M. B.; Snaith, H. J.; Herz, L. M. High Charge Carrier Mobilities and Lifetimes in Organolead Trihalide Perovskites. *Adv. Mater.* **2014**, *26*, 1584−1589.
(3) Shi, D.; Adinolfi, V.; Comin, R.; Yuan, M.; Alarousu, E.; Buin, A.; Chen, Y.; Hoogland, S.; Rothenberger, A.; Katsiev, K.; Losovyj, Y.; Zhang, X.; Dowben, P. A.; Mohammed, O. F.; Sargent, E. H.; Bakr, O. M. Low Trap-State Density and Long Carrier Diffusion in Organolead Trihalide Perovskite Single Crystals. *Science* **2015**, *347*, 519−522.
(4) Xiong, J.; Yang, B.; Wu, R.; Cao, C.; Huang, Y.; Liu, C.; Hu, Z.; Huang, H.; Gao, Y.; Yang, J. Efficient and Non-Hysteresis $CH_3NH_3PbI_3$/PCBM Planar Heterojunction Solar Cells. *Org. Electron.* **2015**, *24*, 106−112.
(5) Xu, W.; Zheng, L.; Zhang, X.; Cao, Y.; Meng, T.; Wu, D.; Liu, L.; Hu, W.; Gong, X. Efficient Perovskite Solar Cells Fabricated by Co Partially Substituted Hybrid Perovskite. *Adv. Energy Mater.* **2018**, *8*, 1703178.
(6) Wang, K.; Zheng, L.; Zhu, T.; Yao, X.; Yi, C.; Zhang, X.; Cao, Y.; Liu, L.; Hu, W.; Gong, X. Efficient Perovskite Solar Cells by Hybrid Perovskites Incorporated with Heterovalent Neodymium Cations. *Nano Energy* **2019**, *61*, 352−360.
(7) National Renewable Energy Laboratory, *Best Research-Cell Efficiency Chart*, https://www.nrel.gov/pv/cell-efficiency.html (accessed: August 2019).
(8) Christians, J. A.; Fung, R. C. M.; Kamat, P. V. An Inorganic Hole Conductor for Organo-Lead Halide Perovskite Solar Cells. Improved Hole Conductivity with Copper Iodide. *J. Am. Chem. Soc.* **2014**, *136*, 758−764.
(9) Zhou, H.; Chen, Q.; Li, G.; Luo, S.; Song, T.-b.; Duan, H.-S.; Hong, Z.; You, J.; Liu, Y.; Yang, Y. Interface Engineering of Highly Efficient Perovskite Solar Cells. *Science* **2014**, *345*, 542−546.
(10) Liu, C.; Wang, K.; Du, P.; Meng, T.; Yu, X.; Cheng, S. Z. D.; Gong, X. High Performance Planar Heterojunction Perovskite Solar Cells with Fullerene Derivatives as the Electron Transport Layer. *ACS Appl. Mater. Interfaces* **2015**, *7*, 1153−1159.
(11) Burschka, J.; Pellet, N.; Moon, S.-J.; Humphry-Baker, R.; Gao, P.; Nazeeruddin, M. K.; Grätzel, M. Sequential Deposition as a Route to High-Performance Perovskite-Sensitized Solar Cells. *Nature* **2013**, *499*, 316−319.
(12) Yao, X.; Qi, J.; Xu, W.; Jiang, X.; Gong, X.; Cao, Y. Cesium-Doped Vanadium Oxide as the Hole Extraction Layer for Efficient Perovskite Solar Cells. *ACS Omega* **2018**, *3*, 1117−1125.
(13) Jeng, J.-Y.; Chiang, Y.-F.; Lee, M.-H.; Peng, S.-R.; Guo, T.-F.; Chen, P.; Wen, T.-C. $CH_3NH_3PbI_3$ Perovskite/Fullerene Planar-Heterojunction Hybrid Solar Cells. *Adv. Mater.* **2013**, *25*, 3727−3732.
(14) Conings, B.; Baeten, L.; De Dobbelaere, C.; D'Haen, J.; Manca, J.; Boyen, H. G. Perovskite-Based Hybrid Solar Cells Exceeding 10% Efficiency with High Reproducibility Using a Thin Film Sandwich Approach. *Adv. Mater.* **2014**, *26*, 2041−2046.
(15) Poorkazem, K.; Liu, D.; Kelly, T. L. Fatigue Resistance of a Flexible, Efficient, and Metal Oxide-Free Perovskite Solar Cell. *J. Mater. Chem. A* **2015**, *3*, 9241−9248.
(16) Kim, B. J.; Kim, D. H.; Lee, Y.-Y.; Shin, H.-W.; Han, G. S.; Hong, J. S.; Mahmood, K.; Ahn, T. K.; Joo, Y.-C.; Hong, K. S.; Park, N.-G.; Lee, S.; Jung, H. S. Highly Efficient and Bending Durable Perovskite Solar Cells: Toward a Wearable Power Source. *Energy Environ. Sci.* **2015**, *8*, 916−921.
(17) Lee, J.-Y.; Connor, S. T.; Cui, Y.; Peumans, P. Solution-Processed Metal Nanowire Mesh Transparent Electrodes. *Nano Lett.* **2008**, *8*, 689−692.
(18) Jeon, I.; Yoon, J.; Kim, U.; Lee, C.; Xiang, R.; Shawky, A.; Xi, J.; Byeon, J.; Lee, H. M.; Choi, M.; Maruyama, S.; Matsuo, Y. High-Performance Solution-Processed Double-Walled Carbon Nanotube Transparent Electrode for Perovskite Solar Cells. *Adv. Energy Mater.* **2019**, *9*, 1901204.
(19) Xia, Y.; Sun, K.; Ouyang, J. Solution-Processed Metallic Conducting Polymer Films as Transparent Electrode of Optoelectronic Devices. *Adv. Mater.* **2012**, *24*, 2436−2440.
(20) Xia, Y.; Sun, K.; Ouyang, J. Highly Conductive Poly (3, 4-Ethylenedioxythiophene): Poly (Styrene Sulfonate) Films Treated with an Amphiphilic Fluoro Compound as the Transparent Electrode of Polymer Solar Cells. *Energy Environ. Sci.* **2012**, *5*, 5325−5332.
(21) Kang, S.; Jeong, J.; Cho, S.; Yoon, Y. J.; Park, S.; Lim, S.; Kim, J. Y.; Ko, H. Ultrathin, Lightweight and Flexible Perovskite Solar Cells with an Excellent Power-Per-Weight Performance. *J. Mater. Chem. A* **2019**, *7*, 1107−1114.
(22) Bryant, D.; Greenwood, P.; Troughton, J.; Wijdekop, M.; Carnie, M.; Davies, M.; Wojciechowski, K.; Snaith, H. J.; Watson, T.; Worsley, D. A Transparent Conductive Adhesive Laminate Electrode for High-Efficiency Organic-Inorganic Lead Halide Perovskite Solar Cells. *Adv. Mater.* **2014**, *26*, 7499−7504.
(23) Li, Z.; Kandel, H. R.; Dervishi, E.; Saini, V.; Biris, A. S.; Biris, A. R.; Lupu, D. Does the Wall Number of Carbon Nanotubes Matter as Conductive Transparent Material? *Appl. Phys. Lett.* **2007**, *91*, 053115.
(24) Cao, W.; Li, J.; Chen, H.; Xue, J. Transparent Electrodes for Organic Optoelectronic Devices: A Review. *J. Photon. Energy* **2014**, *4*, 040990.
(25) Wang, X.; Kyaw, A. K. K.; Yin, C.; Wang, F.; Zhu, Q.; Tang, T.; Yee, P. I.; Xu, J. Enhancement of Thermoelectric Performance of PEDOT: PSS Films by Post-Treatment with a Superacid. *RSC Adv.* **2018**, *8*, 18334−18340.
(26) Kim, N.; Kang, H.; Lee, J.-H.; Kee, S.; Lee, S. H.; Lee, K. Highly Conductive All-Plastic Electrodes Fabricated Using a Novel Chemically Controlled Transfer-Printing Method. *Adv. Mater.* **2015**, *27*, 2317−2323.
(27) Yang, W. S.; Noh, J. H.; Jeon, N. J.; Kim, Y. C.; Ryu, S.; Seo, J.; Seok, S. I. High-Performance Photovoltaic Perovskite Layers Fabricated through Intramolecular Exchange. *Science* **2015**, *348*, 1234−1237.
(28) Zhu, T.; Yang, L.; Liu, L.; Becker, M. L.; Gong, X. Solution-Processed Flexible Broadband Photodetectors with Solution-Processed Transparent Polymeric Electrode. *Adv. Funct. Mater.* **2020**, 1909487.
(29) Yu, Z.; Xia, Y.; Du, D.; Ouyang, J. PEDOT: PSS Films with Metallic Conductivity through a Treatment with Common Organic Solutions of Organic Salts and Their Application as a Transparent

Electrode of Polymer Solar Cells. *ACS Appl. Mater. Interfaces* **2016**, *8*, 11629−11638.
(30) Ouyang, J.; Chu, C.-W.; Chen, F.-C.; Xu, Q.; Yang, Y. High-Conductivity Poly (3, 4-Ethylenedioxythiophene): Poly (Styrene Sulfonate) Film and Its Application in Polymer Optoelectronic Devices. *Adv. Funct. Mater.* **2005**, *15*, 203−208.
(31) Upama, M. B.; Elumalai, N. K.; Mahmud, M. A.; Wang, D.; Haque, F.; Gonçales, V. R.; Gooding, J. J.; Wright, M.; Xu, C.; Uddin, A. Role of Fullerene Electron Transport Layer on The Morphology and Optoelectronic Properties of Perovskite Solar Cells. *Org. Electron.* **2017**, *50*, 279−289.
(32) Zheng, L.; Mukherjee, S.; Wang, K.; Hay, M. E.; Boudouris, B. W.; Gong, X. Radical Polymers as Interfacial Layers in Inverted Hybrid Perovskite Solar Cells. *J. Mater. Chem. A* **2017**, *5*, 23831−23839.
(33) Bi, C.; Wang, Q.; Shao, Y. C.; Yuan, Y. B.; Xiao, Z. G.; Huang, J. S. Non-Wetting Surface-Driven High-Aspect-Ratio Crystalline Grain Growth for Efficient Hybrid Perovskite Solar Cells. *Nat. Commun.* **2015**, *6*, 1−7.
(34) Mastroianni, S.; Heinz, F. D.; Im, J.-H.; Veurman, W.; Padilla, M.; Schubert, M. C.; Würfel, U.; Grätzel, M.; Park, N.-G.; Hinsch, A. Analysing the Effect of Crystal Size and Structure in Highly Efficient $CH_3NH_3PbI_3$ Perovskite Solar Cells by Spatially Resolved Photo-and Electroluminescence Imaging. *Nanoscale* **2015**, *7*, 19653−19662.
(35) Meng, Y.; Ahmadi, M.; Wu, X.; Xu, T.; Xu, L.; Xiong, Z.; Chen, P. High Performance and Stable All-Inorganic Perovskite Light Emitting Diodes by Reducing Luminescence Quenching at PEDOT: PSS/Perovskites Interface. *Org. Electron.* **2019**, *64*, 47−53.
(36) Leonat, L.; Sbarcea, G.; Branzoi, I. V. Cyclic Voltammetry for Energy Levels Estimation of Organic Materials. *UPB Sci. Bull. Ser. B* **2013**, *75*, 111−118.
(37) Sze, S. M.; Ng, K. K. *Physics of Semiconductor Devices*; John Wiley & Sons, 2006.
(38) Sun, K.; Li, P.; Xia, Y.; Chang, J.; Ouyang, J. Transparent Conductive Oxide-Free Perovskite Solar Cells with PEDOT: PSS as Transparent Electrode. *ACS Appl. Mater. Interfaces* **2015**, *7*, 15314−15320.
(39) Wang, K.; Zhang, Z.; Liu, C.; Fu, Q.; Xu, W.; Huang, C.; Weiss, R. A.; Gong, X. Efficient Polymer Solar Cells by Lithium Sulfonated Polystyrene as a Charge Transport Interfacial Layer. *ACS Appl. Mater. Interfaces* **2017**, *9*, 5348−5357.
(40) Wang, K.; Ren, H.; Yi, C.; Liu, C.; Wang, H.; Huang, L.; Zhang, H.; Karim, A.; Gong, X. Solution-Processed Fe_3O_4 Magnetic Nanoparticle Thin Film Aligned by an External Magnetostatic Field as a Hole Extraction Layer for Polymer Solar Cells. *ACS Appl. Mater. Interfaces* **2013**, *5*, 10325−10330.
(41) Liu, C.; Wang, K.; Yi, C.; Shi, X.; Smith, A. W.; Gong, X.; Heeger, A. J. Efficient Perovskite Hybrid Photovoltaics via Alcohol-Vapor Annealing Treatment. *Adv. Funct. Mater.* **2016**, *26*, 101−110.
(42) Street, R.; Schoendorf, M.; Roy, A.; Lee, J. Interface State Recombination in Organic Solar Cells. *Phys. Rev. B: Condens. Matter Mater. Phys.* **2010**, *81*, 205307.
(43) Cowan, S. R.; Roy, A.; Heeger, A. J. Recombination in Polymer-Fullerene Bulk Heterojunction Solar Cells. *Phys. Rev. B: Condens. Matter Mater. Phys.* **2010**, *82*, 245207.
(44) Xu, W.; Yao, X.; Meng, T.; Wang, K.; Huang, F.; Gong, X.; Cao, Y. Perovskite Hybrid Solar Cells with a Fullerene Derivative Electron Extraction Layer. *J. Mater. Chem. C* **2017**, *5*, 4190−4197.
(45) Li, Z.; Wang, W.; Greenham, N. C.; McNeill, C. R. Influence of Nanoparticle Shape on Charge Transport and Recombination in Polymer/Nanocrystal Solar Cells. *Phys. Chem. Chem. Phys.* **2014**, *16*, 25684−25693.
(46) Koster, L. J. A.; Mihailetchi, V. D.; Ramaker, R.; Blom, P. W. M. Light Intensity Dependence of Open-Circuit Voltage of Polymer: Fullerene Solar Cells. *Appl. Phys. Lett.* **2005**, *86*, 123509.
(47) Zhu, T.; Zheng, L.; Xiao, Z.; Meng, X.; Liu, L.; Ding, L.; Gong, X. Functionality of Non-Fullerene Electron Acceptors in Ternary Organic Solar Cells. *Solar RRL* **2019**, *3*, 1900322.

https://dx.doi.org/10.1021/acsami.9b22891
ACS Appl. Mater. Interfaces XXXX, XXX, XXX−XXX